Linearly and circularly polarized radiation with a low on-axis heat load from an asymmetric magnet pole undulator

Zhouyu Zhao🟢 and Qika Jia🔵*

National Synchrotron Radiation Laboratory, University of Science and Technology of China, Hefei, 230029, Anhui, People's Republic of China

The heavy heat load on optical components from the normal planar undulator has become a serious problem in the synchrotron radiation light source, especially for generating the low-energy photon in a high-energy storage ring and/or a diffraction-limited storage ring. The asymmetric magnet pole undulators have different period lengths between the upper and lower magnet poles. Taking the advantage of the asymmetric magnet pole undulators in building various magnetic fields, this paper proposes a new class of undulators to obtain the specific magnetic fields which can scatter the electron velocity away from the undulator axis. It consists of four magnet arrays and has a similar structure compared to the DELTA/ APPLE-X undulator; however, each couple of magnet arrays has a different period length with the period ratio of $n_1 : n_2$. Taking the one-to-two and two-to-three period ratios as examples, a novel Figure 8 undulator and a novel Knot undulator are demonstrated. The polarization state can be flexibly switched from the linear polarization to the circular polarization by tuning the phase shifts of magnetic fields, with the on-axis heat load greatly suppressed. The heat-load suppressions of linear polarization at two predetermined orthogonal directions are almost the same and fully effective. Analysis and simulations of undulator designs with the corresponding radiation characteristics are reported.

I. INTRODUCTION

One of the most important features of the diffraction-limited storage ring (DLSR) is the extremely low emittance, which is particularly beneficial to enhancing the photon brightness and flux density [1–3]. For the circularly polarized undulator, the horizontal and vertical magnetic fields have a constant phase shift of $\pi/2$. Since the electron velocity is always scattered away from the undulator axis, the circular radiation has little on-axis heat load. In contrast, the heat load from a normal planar undulator becomes a serious problem in the optical components of the beam line, especially for generating the low-energy photon in a high-energy storage ring and/or a DLSR.

To reduce the on-axis heat load of the linearly polarized radiation from a normal planar undulator, different types of undulators have been proposed and studied, including Figure 8 undulator [4–8], Leaf undulator [9,10], and APPLE-Knot undulator [11–14]. Most of them have several groups of magnet arrays to generate the horizontal and vertical magnetic fields. The horizontal and vertical fields are alternately advanced with a constant phase shift, then the circularly polarized radiations with the opposite rotation directions can be mutually canceled, thus the linearly polarized radiation with a low heat load can be obtained. However, the usual Figure 8 undulator can only deliver the linear radiation. The usual Leaf undulator seems can realize an arbitrary polarization state by energizing the coil with different patterns, but in the linear mode its heat load only can be suppressed around 45° linear polarization. The polarization switching is complicated and the hysteresis is also harmful in practice. The APPLE-Knot undulator is capable to deliver arbitrarily polarized radiation. Since its period lengths are of two-to-three ratio, both the linearly and circularly polarized radiation can achieve a high polarization degree. Contrary to the Leaf undulator, the APPLE-Knot undulator has a strong ability to suppress the heat load for both the horizontally and vertically linear polarization but is incapable to suppress the heat load around 45° linear polarization. The usual APPLE-Knot undulator has a complicated magnet structure that consists of eight magnet arrays. For the latest proposed APPLE-Knot undulator, the number of magnet arrays is decreased from 8 to 4 by magnetizing the pole with a tilt angle. However, the correction of field error and magnet shimming will be challenging and possibly constitute an obstacle to carrying on such an undulator in practice, especially for a DLSR [15]. In general, the above low

heat-load undulators based on the APPLE-type undulator have an innate defect that the horizontal field is weaker than the vertical field, which results in a relatively weak heat-load suppression for the vertically polarized radiation.

In a previous publication for a planar undulator, we have proposed the asymmetric magnet pole undulator (AMPU), in which the upper and lower magnet poles have different period lengths [16]. The AMPU has a good potential to build different types of magnetic fields and then obtain various undulator radiations. The previous study shows that the planar AMPU also can suppress the on-axis heat load to some extent, whereas a portion of heat load still exists on the axis.

In this paper, benefiting from the advantage of AMPU in building various magnetic fields, we propose a new class of undulators to greatly suppress the on-axis heat load by applying the AMPU concept to both the horizontal and vertical directions. The proposed undulator consists of two orthogonal couples of magnet arrays. Its transverse structure is similar to the DELTA/APPLE-X undulator and is simpler than the APPLE-type low heat-load undulator, which is based on the APPLE II undulator and has the additional magnet arrays on both sides. [17–20]. By setting a different period length in two orthogonal directions, various magnetic fields can be realized, such as obtaining a constant phase shift or an alternately varied phase relation between the magnetic fields in two directions. Taking the one-to-two and two-to-three period ratios as examples, a novel Figure 8 field mode and a novel Knot field mode can be obtained in this method. It enables us to realize arbitrarily polarized radiation. The polarization state can be flexibly switched from the linear to circular polarization by tuning the phase shifts, with the on-axis heat load greatly suppressed. The transverse structure arranged with the DELTA/APPLE-X structure leads to the same magnetic field strength in two orthogonal directions, which then ensures the effectiveness of heat-load suppression.

The rest of this paper is organized as follows: Sec. II introduces the principles of the proposed undulators. Then in Sec. III, the undulator designs and the corresponding radiation characteristics are numerically studied for the novel Figure 8 undulator and the novel Knot undulator. Some features of the proposed undulators are discussed in Sec. IV. Finally Sec. V gives a summary. The derived equations of electron motion in the proposed undulators are given in the Appendix.

II. PRINCIPLES

From the perspective of electron motion, the key to reduce the on-axis heat load is to make sure the electron velocity is always deviated from the undulator axis. Obviously, the elliptically polarized undulator (EPU) can fully satisfy this condition when it works in the elliptical mode. In contrast, the linear mode of EPU and the normal planar undulator probably have a heavy on-axis heat load.

From the perspective of magnetic field, to reduce the on-axis heat load of the linear mode of APPLE-type undulators, the horizontal and vertical magnetic fields should be alternately advanced with a constant phase shift. The circular polarization is canceled then the sum of radiations will be linearly polarized with the little on-axis heat load. Most of the APPLE-type low heat-load undulators follow this basic principle and use several groups of magnet arrays to form the required magnetic fields. By setting the horizontal and vertical magnetic fields with the different period lengths, the on-axis heat load can be effectively suppressed. Taking a typical Figure 8 undulator and a typical APPLE-Knot undulator as examples, the horizontal and vertical period lengths have a one-to-two period ratio and two-to-three period ratio, as shown in Fig. 1. Under these conditions, the ideal expressions of the typical magnetic fields for the linearly polarized radiation are given as

$$B_y = B_{y0} \, \sin\left(\frac{2\pi}{n_1 \lambda_{\mathrm{u}}} z\right)$$
$$B_x = B_{x0} \, \sin\left(\frac{2\pi}{n_2 \lambda_{\mathrm{u}}} z + \phi_0\right), \tag{1}$$

where B_{y0} and B_{x0} are the on-axis amplitudes of magnetic fields, λ_{u} is the unit period length, ϕ_0 is the phase shift, (n_1, n_2) equals (1,2) and (2,3) and corresponds to the Figure 8 undulator and the APPLE-Knot undulator, respectively.

The typical electron orbits and velocities for Figure 8 undulator and APPLE-Knot undulator are shown in Figure 2. The electron orbit in the Figure 8 undulator has an eight-figure shape, while in the APPLE-Knot undulator the electron moves as a complex knot-figure shape. The electron moves as the right-hand circle and left-hand circle alternately, which results in the cancelation of circular polarization. Only the linearly polarized radiation is preserved on the axis. Figures 2(b) and 2(d) indicate that the electron velocity is always deviated from the undulator axis, thus the on-axis heat load can be greatly suppressed. To generate the circularly polarized radiation in the APPLE-Knot undulator, both the inner and outer APPLE
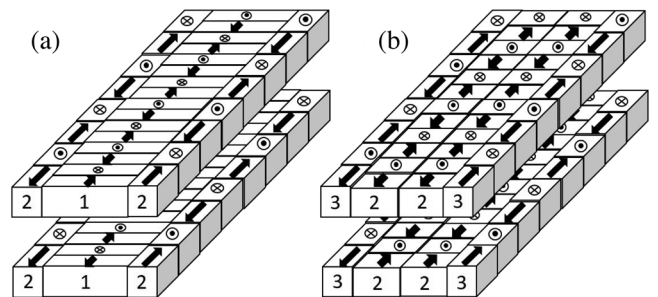
FIG. 1. Schematic illustrations of (a) the typical Figure 8 undulator and (b) the typical APPLE-Knot undulator.
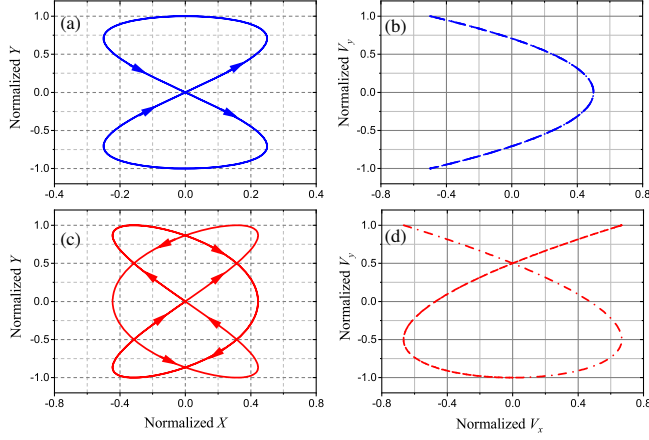
FIG. 2. The electron orbits (solid left) and velocities (dotted right) in the x-y plane, in which the upper subfigures (blue) and lower subfigures (red) are corresponding to the Figure 8 undulator and the linear mode of APPLE-Knot undulators, respectively.

arrays should be adjusted to work in the circular mode, which is similar to the normal APPLE-II undulator [13].

Here we propose a new class of undulators by applying the AMPU concept to the DELTA/APPLE-X-type undulator. As shown in Fig. 3(a), it has four magnet arrays, in which the top and right magnet arrays have period length $n_1 \lambda_u$ while the bottom and left magnet arrays have period length $n_2 \lambda_u$. Different period lengths can be found in both field directions. Comparing the Fig. 1 with Fig. 3(a), we can find that the difference between the proposed undulator and the typical Fig. 8/APPLE-Knot undulator is particularly obvious. Since the magnetic field of the pure-permanent magnet undulator can be regarded as the superimposition of magnetic waves from each magnet pole, the magnetic fields can be described as

$$
\begin{aligned}
B_y &= B_1 \, \sin\left(\frac{2\pi}{n_1 \lambda_u} z + \phi_1\right) + B_2 \, \sin\left(\frac{2\pi}{n_2 \lambda_u} z + \phi_2\right) \\
B_x &= B_1 \, \sin\left(\frac{2\pi}{n_1 \lambda_u} z + \phi_3\right) + B_2 \, \sin\left(\frac{2\pi}{n_2 \lambda_u} z + \phi_4\right),
\end{aligned} \quad (2)
$$
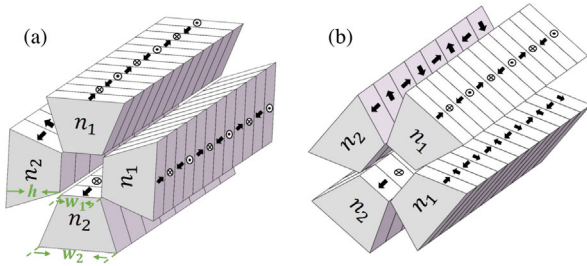
FIG. 3. Schematic illustrations of the proposed AMPU under DELTA-type (a) and APPLE-X-type (b) transverse structures with the period ratio $n_1 : n_2$ at each direction.

where B_1 and B_2 are the on-axis amplitudes of magnetic fields from the upper (right) and lower (left) magnet poles, respectively, and ϕ_{1-4} are the phase shifts. Different types of undulators can be achieved by changing the period ratio $n_1 : n_2$. Here the magnet poles are arranged with the DELTA-type/APPLE-X-type structure. From the left side to the right side of Fig. 3, the transverse structure is rotated by the angle of 45°. Obviously, the corresponding transverse distribution of the polarization state is also rotated, thus different functions can be achieved with these two types of transverse structures in the proposed undulators.

According to the magnetic fields above, we can solve the equations of electron motions, then derive the distributions of photon flux and radiation power based on the Lienard-Wiechert potential of a point charge. The flux density and power density can be calculated by [21]

$$
\frac{\mathrm{d}^2 F}{\mathrm{d}\Omega \mathrm{d}\omega} = \frac{I e \omega^2}{16 \pi^3 \varepsilon_0 c} \left| \int_{-\infty}^{\infty} \mathbf{n} \times (\mathbf{n} \times \boldsymbol{\beta}) e^{i\omega(t - \mathbf{n} \cdot \mathbf{r}/c)} \mathrm{d}t \right|^2, \quad (3)
$$

$$
\frac{\mathrm{d}^2 P}{\mathrm{d}\Omega \mathrm{d}t} = \frac{I e}{16 \pi^2 \varepsilon_0 c} \frac{|\mathbf{n} \times [(\mathbf{n} - \boldsymbol{\beta}) \times \dot{\boldsymbol{\beta}}]|^2}{(1 - \mathbf{n} \cdot \boldsymbol{\beta})^5}, \quad (4)
$$

where I is the average beam current, $\mathbf{n}$ is the unit vector from the electron position to the observation direction, $\boldsymbol{\beta}$ is the vector of relative velocity, $\dot{\boldsymbol{\beta}}$ is the acceleration vector and $\mathbf{r}$ is the vector from the electron position to the observation position. With the calculated photon flux, the polarization degrees can be calculated by

$$
\begin{aligned}
P_L &= \frac{|F_x|^2 - |F_y|^2}{|F_x|^2 + |F_y|^2}. \\
P_C &= \frac{2\mathrm{Im}(F_x F_y^*)}{|F_x|^2 + |F_y|^2}. \\
P_{45} &= \frac{2\mathrm{Re}(F_x F_y^*)}{|F_x|^2 + |F_y|^2}.
\end{aligned} \quad (5)
$$

The proposed undulator has a large number of variables, especially for a variable period ratio, thus it is possible for us to obtain various magnetic fields, then realize different specific radiation features. Inspired by the typical Fig. 8/APPLE-Knot undulator and based on AMPU, a novel Figure 8 field and a novel Knot field can be obtained by setting the one-to-two and two-to-three period ratios with the optimized phase shifts and field amplitudes. In these two field modes, the on-axis heat load can be greatly suppressed both for the linear polarization and circular polarization. The detailed information on electron motion in the proposed undulators is derived in the Appendix.

III. UNDULATOR DESIGN AND RADIATION CHARACTERISTIC

Following the principles demonstrated above, the main parameters of the proposed undulator, such as the phase shifts and the field amplitudes, are optimized and determined by the radiation characteristics calculated from the above equations and simulated based on SPECTRA [22]. The undulators are designed by *RADIA* [23]. The magnetic material is NdFeB with a remanence of 1.32 T. All the calculations shown in this paper are referenced to the parameters of the Hefei Advanced Light Facility (HALF), a 2.2 GeV DLSR proposed by the National Synchrotron Radiation Laboratory in China [24]. In the undulator design, first, the undulator strength parameter and unit period length are determined by the target photon energy. Then we optimize the field amplitudes and the phase shifts by referring to the field waveforms of the typical Figure 8 undulator and APPLE-Knot undulator. In the linear polarization mode, the horizontal and vertical fields should be advanced alternately, while in the circular polarization mode, the horizontal and vertical fields have a constant phase relation. To obtain the required phase relation between the horizontal and vertical fields, the field amplitudes from a couple of magnet arrays should not be too close. The magnetic field is further optimized by the radiation performance, especially for the polarization degree and the on-axis radiation power under different polarization modes. In addition, note that the field amplitude is limited by the actual condition of the undulator, such as the remanence of magnetic material, the minimum undulator gap, and so on.

A. Figure 8 AMPU

In the Fig. 8 AMPU, the period ratio is set to 1∶2. To reach the fundamental photon energy around 7 eV, the unit length of the undulator period is set to 70 mm, thus the period lengths of one couple of magnet arrays are 70 and 140 mm, respectively. Let us first consider the case of the DELTA-type undulator without 45° rotation, as shown in Fig. 3(a). The three-dimensional sizes of the magnet pole are set with $h = 32$ mm, $w_1 = 10$ mm, and $w_2 = 42$ mm. The optimal magnetic fields of the linear and circular polarization modes are given as

$$B_y(\text{T}) = 0.26 \sin\left(\frac{2\pi}{70}z - \frac{5\pi}{8} \pm \frac{\pi}{8}\right)$$

$$+ 0.49 \sin\left(\frac{2\pi}{140}z \pm \frac{3\pi}{4}\right)$$

$$B_x(\text{T}) = 0.26 \sin\left(\frac{2\pi}{70}z + \frac{\pi}{2}\right)$$

$$+ 0.49 \sin\left(\frac{2\pi}{140}z + \frac{3\pi}{4}\right). \qquad (6)$$

Since the field amplitudes contributing from each magnet array are 0.26 and 0.49 T, the magnet arrays with different period lengths should have different half gaps. The distance from the beam axis to the upper (right) array with a period length of 70 mm is about 11 mm, while the distance between the axis and the lower (left) array with a period length of 140 mm is set to about 6.7 mm. The field mode switching from the linear polarization to circular polarization is realized by changing the phase shifts of one couple of magnet poles at the vertical direction while another couple of magnet poles at the horizontal direction are fixed. Figure 4 shows the magnetic fields, electron orbits and electron velocities. Table I summarizes the settings of phase shifts of different polarization modes. In the linear polarization mode, the phase shifts of two magnet poles of B_y are set to $-\pi/2$ and $3\pi/4$, which are corresponding to -17.5 and 52.5 mm, respectively. The phase shifts of B_x are set to $\pi/2$ (17.5 mm) and $3\pi/4$ (52.5 mm). We can find that B_y and B_x are alternately advanced with a constant phase shift. The electron moves in a tilt eight-figure shape and its velocity is always larger than zero, thus most of the heat load is scattered away from the axis. In the circular polarization mode, the phase shifts of B_y are both set to $-3\pi/4$, which are corresponding to -26.25 and -52.5 mm, respectively. The phase shifts of B_x
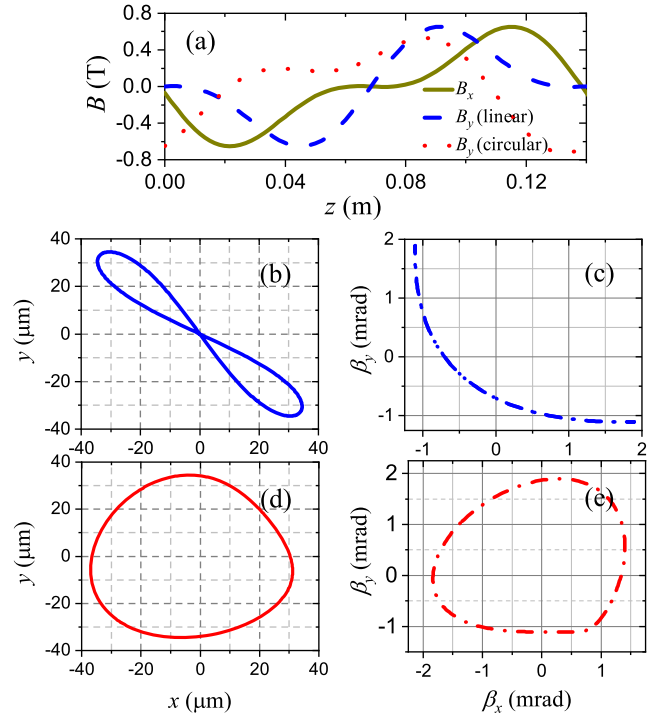
FIG. 4. The magnetic fields (a) of the linear and circular mode in the Fig. 8 AMPU, with the corresponding electron orbits (b), (d) and velocities (c), (e). The blue lines (b), (c) are corresponding to the 135° linear mode and the red lines (d), (e) are corresponding to the right-hand circular mode, respectively.

TABLE I.   Phase shifts of magnet arrays for different polarization modes in the Fig. 8 AMPU.

	Upper	Lower	Right	Left
Polarization mode	ϕ_1	ϕ_2	ϕ_3	ϕ_4
45° linear	$\pi/2$	$-\pi/4$	$\pi/2$	$3\pi/4$
135° linear	$-\pi/2$	$3\pi/4$	$\pi/2$	$3\pi/4$
Left circular	$-3\pi/4$	$\pi/4$	$\pi/2$	$3\pi/4$
Right circular	$-3\pi/4$	$-3\pi/4$	$\pi/2$	$3\pi/4$

are the same as that of the linear mode. On this condition, B_x always advances B_y with a constant phase shift, thus the undulator works in the circular mode. The electron moves as a circle shape approximately and its velocity is deviated from the zero point with a larger amplitude than the linear mode. We can predict that the circular mode should have a better performance on the heat-load suppression than the linear mode.

Based on the optimized magnetic fields above, the corresponding radiation characteristics for the linearly and circularly polarized modes are studied in detail, as shown in Fig. 5. The peak flux is optimized around the photon energy of 7 eV with undulator length set to about 2 m and pinhole radius setting to 0.3 mrad. The calculation results based on Eqs. (3) and (5) show a good consistency with the simulation results from SPECTRA. The linear and circular polarization degrees at 7 eV reach 99.4% and 99.9%, respectively, which are almost the same as the normal planar undulator and EPU. The photon flux of circular mode is 2 times larger than the linear mode at 7 eV. Note that here the undulator radiation at linear mode is 135° linearly polarized and its polarization degree at high harmonic is lower than that at fundamental photon energy. The high harmonic of linear mode has a considerable photon flux, however, the polarization degree reduces sharply. At the fifth harmonic, the polarization degree is reduced to 45%. Only the flux at fundamental photon energy is useful if the users require a high polarization degree. In contrast, the high harmonic of circular mode is always larger than 95%, but the corresponding flux is greatly reduced.

For the optical beam with low photon energy and the electron beam with a standard transverse Gaussian distribution at HALF, the divergence σ_r' is close to the diffraction limit, which is roughly determined by $\sqrt{\lambda_s/2L}$ with λ_s being the radiation wavelength and L being the undulator length. In a pinhole with a radius of 0.4 mrad ($2\sigma_r'$), more than 95% of the photons are collected. Figure 6 shows the photon flux and polarization degree depend on pinhole radius at 7 eV. With the increase of pinhole radius, the photon flux is also increased with a decreased polarization degree. The flux reaches the maximum when the radius is larger than 0.4 mrad. The polarization degrees for these two modes are both on the level of 99% within the
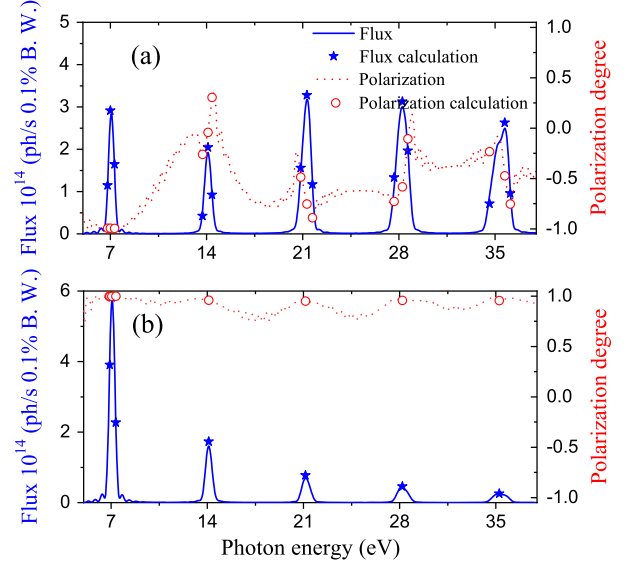
FIG. 5.   The photon flux (solid blue) and polarization degree (dotted red) depend on photon energy for the linear mode (a) and the circular mode (b) in the Fig. 8 AMPU, with the pinhole radius of 0.3 mrad. The lines are from the SPECTRA code and the scatter symbols are based on Eqs. (3) and (5).

pinhole radius of 0.4 mrad. Even if the radius is increased to 1 mrad, the circular mode still can reach the polarization degree of 99.3% while the polarization degree of linear mode is about 97.6%.

The power distributions of these two modes are shown in Fig. 7. We can find that most of the heat load is scattered away from the axis. Within the pinhole radius of 0.3 mrad, the on-axis heat load of the linear mode is about 7.84 W while the circular mode only has 0.10 W heat load on the axis. The corresponding theoretical results from Eq. (4) are
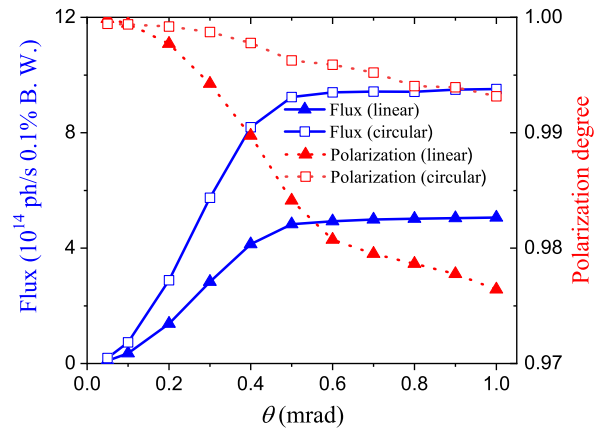
FIG. 6.   The photon flux (solid blue) and polarization degree (dotted red) depend on pinhole radius at 7 eV for the linear mode (triangle symbol) and circular mode (square symbol) in the Fig. 8 AMPU.
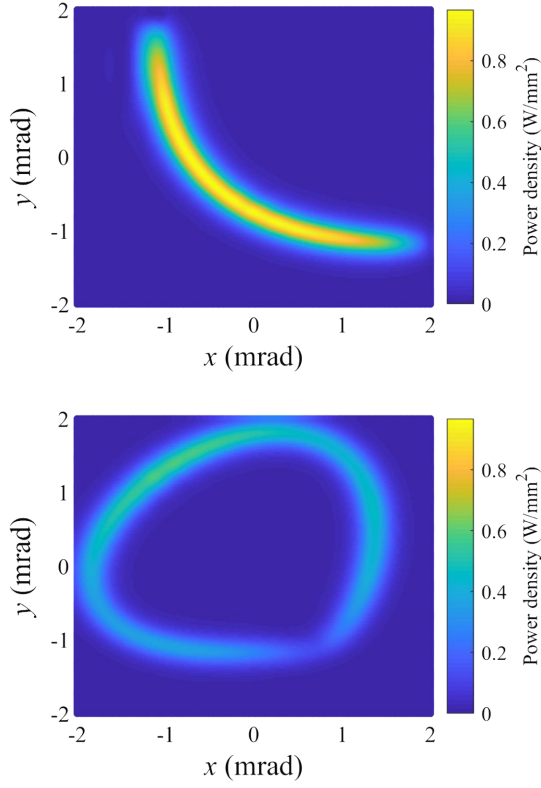
FIG. 7. The transverse distribution of power density for the linear mode (upper) and circular mode (lower) in the Fig. 8 AMPU.

equal to 8.53 and 0.11 W, respectively, which are almost the same as the simulation results. Though the heat load of the linear mode is more than an order of magnitude larger than the circular mode, the on-axis heat load of both of the two modes is effectively suppressed in comparison to the normal planar undulator, whose heat load is on the level of hundreds to thousands of watts.

The polarization state of the Fig. 8 AMPU can be easily switched by changing the phase shift. In the linear mode, the polarization angle can be switched from 135° to 45° by changing the phase shifts of B_y from $-\pi/2$, $3\pi/4$ (-17.5 and 52.5 mm) to $\pi/2$, $-\pi/4$ (17.5 and -17.5 mm). The 45° linear polarization degree can reach 99.4% with a low on-axis heat load (7.74 W @ 0.3 mrad). The circular mode also can be easily switched from the right-circular polarization to left-circular polarization by changing the lower phase shift of B_y from $-3\pi/4$ (-52.5 mm) to $\pi/4$ (17.5 mm), while keeping the upper phase shift constant. The corresponding polarization degree can reach 99.9% and the on-axis heat load is about 0.27 W within 0.3 mrad pinhole. In addition, the horizontal and vertical polarization states also can be obtained if we open the undulator gap in one direction. On this condition, the on-axis heat load will be similar to the normal planar undulator and cannot be suppressed.

TABLE II. Phase shifts of magnet arrays for different polarization modes in the Knot AMPU.

	Upper	Lower	Right	Left
Polarization mode	ϕ_1	ϕ_2	ϕ_3	ϕ_4
45° linear	$-\pi/4$	$-\pi/2$	$-\pi/4$	$\pi/2$
135° linear	$3\pi/4$	$\pi/2$	$-\pi/4$	$\pi/2$
Left circular	$-11\pi/12$	$\pi/18$	$-\pi/4$	$\pi/2$
Right circular	$\pi/3$	$8\pi/9$	$-\pi/4$	$\pi/2$

B. Knot AMPU

Similar to the Fig. 8 AMPU, a novel Knot undulator can be realized by setting the period ratio $n_1 : n_2$ with $2:3$ in each direction. Here the unit length of the undulator period is set to 48 mm, thus the period lengths of one couple of magnet arrays are 96 and 144 mm, respectively. In this section, we also first consider the case of the DELTA-type undulator. The three-dimensional sizes of the magnet pole are set with $h = 35$ mm, $w_1 = 18$ mm, and $w_2 = 54$ mm. The fundamental photon energy is also chosen at around 7 eV, and the optimal magnetic fields of the linear and circular polarization modes are given as
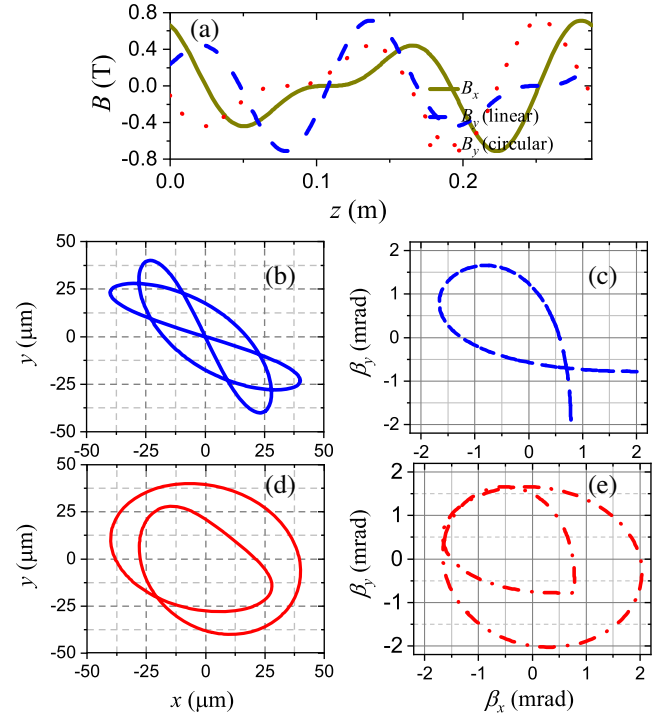
FIG. 8. The magnetic fields (a) of the linear and circular mode in the Knot AMPU, with the corresponding electron orbits (b), (d) and velocities (c), (e). The blue lines (b), (c) are corresponding to the 135° linear mode and the red lines (d), (e) are corresponding to the right-hand circular mode, respectively.

$$B_y(\text{T}) = 0.3 \, \sin\left(\frac{2\pi}{96}z + \frac{13\pi}{24} \pm \frac{5\pi}{24}\right)$$
$$+ 0.45 \, \sin\left(\frac{2\pi}{144}z + \frac{25\pi}{36} \mp \frac{7\pi}{36}\right)$$
$$B_x(\text{T}) = 0.3 \, \sin\left(\frac{2\pi}{96}z - \frac{\pi}{4}\right)$$
$$+ 0.45 \, \sin\left(\frac{2\pi}{144}z + \frac{\pi}{2}\right). \qquad (7)$$

The field amplitudes contributing from each magnet array are 0.3 and 0.45 T. The distance from the beam axis to the upper (right) array with a period length of 96 mm is about 13.3 mm, while the distance between the axis and the lower (left) array with a period length of 144 mm is set to about 10.4 mm. The polarization switching is also realized by changing the phase shifts of one couple of magnet poles at the vertical direction and keeping another couple of magnet poles at a horizontal direction fixed. The magnetic fields, electron orbits and electron velocities are shown in Fig. 8. Table II summarizes the settings of phase shifts of different polarization modes. In the linear polarization mode, the phase shifts of two magnet poles of B_y are set to $3\pi/4$ and $\pi/2$, which are both equal to 36 mm. The phase shifts of B_x are set to $-\pi/4$ (-12 mm) and $\pi/2$ (36 mm). The electron moves as a tilt complex knot-figure shape and its velocity is always larger than zero, thus most of the heat load is scattered away from the axis. In the circular polarization mode, the phase shifts of B_y are set to $\pi/3$ and $8\pi/9$, which are corresponding to 16 and 64 mm, respectively. The phase shifts of B_x are the same as that of the linear mode. The electron moves as a double ellipse approximately and its velocity is also deviated from the zero point.

Then we also study the radiation characteristics based on the optimized magnetic fields given above. Figure 9 shows the photon flux and polarization degree of the linearly and circularly polarized modes in the Knot AMPU. The peak flux is optimized around the photon energy of 7 eV with undulator length set to about 2 m and pinhole radius set to 0.3 mrad. The linear and circular polarization degrees at 7 eV are 99.1% and 99.3%, respectively, which are almost the same as the Fig. 8 AMPU. The photon flux of the linear mode is almost the same as the circular mode at 7 eV. Unlike the novel Figure 8 undulator, with the increase of harmonic order, the linear polarization angle of the novel Knot undulator is alternately switched between 135° and 45°, while the circular polarization angle is fixed. Furthermore, the novel Knot undulator has abundant harmonic radiation both for the two modes. The harmonic can keep a high polarization degree, which is benefiting from a two-to-three period ratio that introduces a small coupling among the harmonics. Thus the novel Knot undulator has more usable harmonics than the novel Figure 8 undulator. However, the photon flux of this
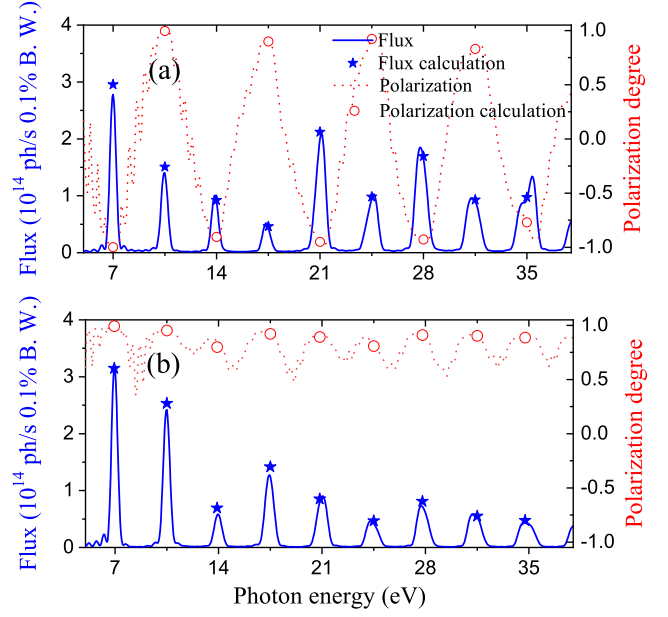
FIG. 9. The photon flux (solid blue) and polarization degree (dotted red) depend on photon energy for the linear mode (a) and the circular mode (b) in the Knot AMPU, with the pinhole radius of 0.3 mrad. The lines are from SPECTRA code and the scatter symbols are based on Eqs. (3) and (5).

Knot undulator is slightly lower than the Figure 8 undulator. It is due to a comparatively large period length and a comparatively small magnetic field in the Knot AMPU. The photon flux and polarization degree depend on pinhole radius at 7 eV as shown in Fig. 10. The flux also reaches the maximum when the radius is larger than 0.4 mrad. The polarization degrees of these two modes are both on the level of 99% within the pinhole radius of 0.4 mrad.

The power distributions of these two modes are shown in Fig. 11. Within the pinhole radius of 0.3 mrad, the on-axis heat load of the linear mode is about 7.36 W while the
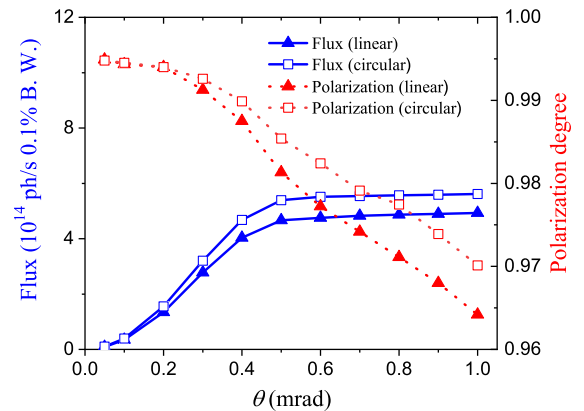
FIG. 10. The photon flux (solid blue) and polarization degree (dotted red) depend on pinhole radius at 7 eV for the linear mode (triangle symbol) and circular mode (square symbol) in the Knot AMPU.
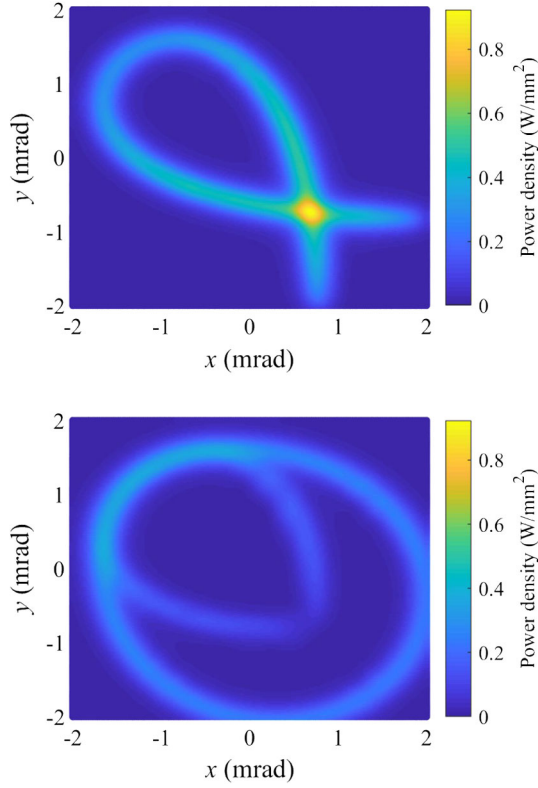
FIG. 11. The transverse distribution of power density for the linear mode (upper) and circular mode (lower) in the Knot AMPU.

circular mode only has 0.54 W heat load on the axis. Most of the heat load is scattered away from the axis. The simulation results are consistent with the on-axis heat load calculated by Eq. (4), which is equal to 7.74 and 0.52 W, respectively. Thus the on-axis heat load in this novel Knot undulator can be greatly suppressed. The same as the novel Figure 8 undulator, in fixed photon energy, the polarization state of the novel Knot undulator also can be switched by changing the phase shifts. In the linear mode, the polarization angle can be switched from 135° to 45° by changing the phase shifts of B_y from $3\pi/4$, $\pi/2$ (36 and 36 mm) to $-\pi/4$, $-\pi/2$ (-12 and -36 mm). The 45° linear polarization degree can reach 99.1% with a low on-axis heat load (7.37 W @ 0.3 mrad). In the circular mode, the polarization angle can be switched from the right-circular polarization to left-circular polarization by changing the phase shifts of B_y from $\pi/3$, $8\pi/9$ (16 and 64 mm) to $-11\pi/12$, $\pi/18$ (-44 and 4 mm). The corresponding polarization degree reaches 99.9% and the on-axis heat load is about 0.43 W within the pinhole radius of 0.3 mrad.

The above study is focused on the DELTA-type undulator, which can be converted into the APPLE-X-type undulator by rotating the transverse structure with an angle of 45°. The 45° and 135° linear polarization will become the horizontal and vertical linear polarization, respectively. The radiation performance in the proposed novel Fig. 8 and

Knot undulator will be similar to the original Fig. 8 and APPLE-Knot undulator, but with a higher polarization degree and a lower on-axis heat load, especially for 135°/vertically polarized radiation.

IV. DISCUSSIONS

The proposed undulators are based on AMPU with the arrangement of the DELTA/APPLE-X structure. Considering the case that the DELTA-type/APPLE-X-type undulator has a variable gap [19,20], if one wants to change the photon energy with the specific radiation feature in the proposed undulators, at least one couple of magnet arrays should be capable of independently tuning both the undulator gaps and phase shifts, while the phase shifts of another couple of magnet arrays can be fixed. Since the period lengths and the magnetic contributions from each magnet array are both quite different, the beam axis should be deviated from the undulator geometric center. Thus an elaborate optimization of the undulator gap is necessary. We can find that the proposed AMPU is quite different with the traditional APPLE/APPLE II undulator on the beam axis. The same as the DELTA-type/APPLE-X-type undulator, it will bring some benefits in tuning the magnetic field with more degrees of freedom than the other types of undulators, which probably enables the experiment users to obtain the best magnetic field profile according to the detected radiation characteristics. In addition, if we open the undulator gap to increase the fundamental photon energy, a reduced magnetic field will make the transverse velocity close to the beam axis, which weakens the performance of the on-axis heat-load suppression. However, the total power of the undulator is proportional to the square of field amplitude and the power density is proportional to the field amplitude. With the increase of undulator gap, the total power reduces sharply with the on-axis power decreasing synchronously. In this condition, the on-axis heat-load problem is greatly relaxed, the optical components of beam line are possible to overcome the on-axis heat load even without a low on-axis heat-load undulator. Therefore a low on-axis heat load can be always obtained under different undulator gaps, while the other radiation characteristics can be maintained if changing the undulator gap with a constant field amplitude ratio.

The proposed undulators are optimized with the specific field amplitude and phase shift. As demonstrated above, the electron velocity is always deviated from the zero point with a certain distance, thus the radiation characteristics should not be sensitive to these parameters. Since the phase shifts of B_x are fixed at these two novel undulators, here we only consider the deviation of the phase shift of B_y. Actually, the deviation of phase shift is the relative difference between a couple of magnet arrays, thus here the radiation characteristics are studied by taking the deviation of ϕ_2 as an example and keeping ϕ_1 constant, as shown in Fig. 12. The resonant photon energy is independent of the
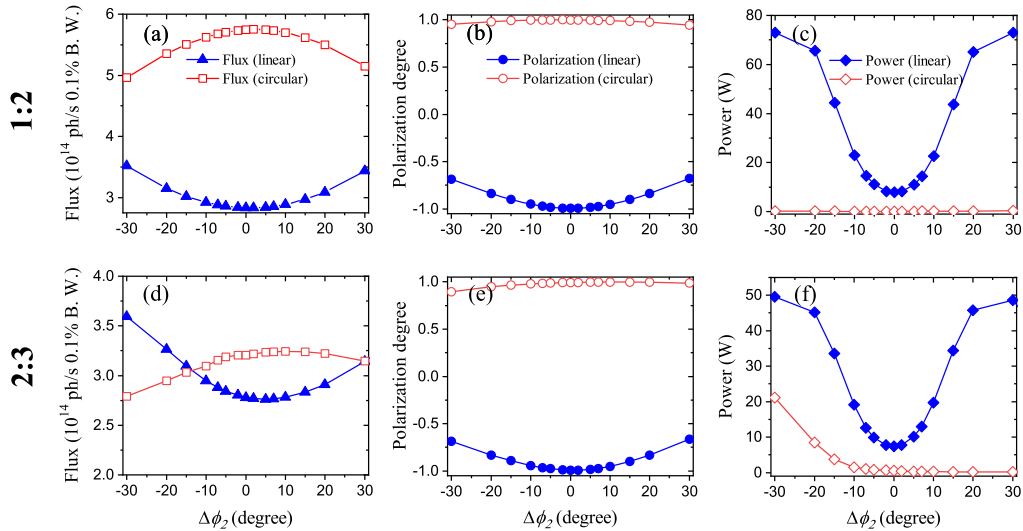
FIG. 12. The flux (left), polarization degree (middle) and power (right) depend on the deviation of phase shift ϕ_2. Upper subfigures are corresponding to the Fig. 8 AMPU and lower subfigures are corresponding to the Knot AMPU, respectively.

phase shift. Within the range of $\pm 7°$ degree, the flux changes little and the radiation power still can be effectively suppressed. The circular mode can always keep a high polarization degree in these two novel undulators, but the polarization degree of linear mode is a little sensitive to $\Delta \phi_2$. With $\Delta \phi_2$ increasing from $0°$ to $\pm 7°$, the circular polarization degree is still on the level of 99% while the linear polarization degree is decreased from 99% to 97%. In practice, $\Delta \phi$ can be easily limited within the range of $\pm 1°$.

We further study the sensibility of radiation characteristics on the field amplitude, as shown in Fig. 13. Here we also select the deviation of field amplitude B_2 as an

example and keep the other field amplitudes constant. In a large range of $\Delta B_2/B_2$, the polarization degree and radiation power have little changes. Within the range of $|\Delta B_2/B_2| < 0.1$, the polarization degree is almost on the level of 99%, and the power is always lower than 10 W. Considering that the beam axis is asymmetric with respect to the upper (right) and lower (left) arrays of undulators, it will be beneficial for us to select the beam orbit which can always realize an effective heat-load suppression and keep a high polarization degree. However, unlike the phase shift, the resonant photon energy is dependent on the field amplitude. With the increase of $\Delta B_2/B_2$, the resonant photon energy is slightly decreased, and the photon flux
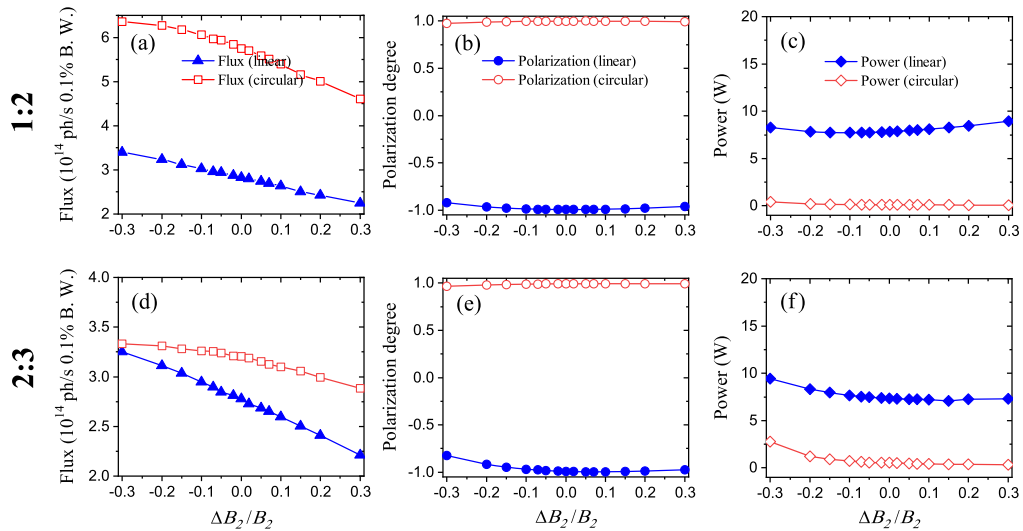
FIG. 13. The flux (left), polarization degree (middle) and power (right) depend on the deviation of field amplitude B_2. Upper subfigures are corresponding to the Fig. 8 AMPU and lower subfigures are corresponding to the Knot AMPU, respectively.

also will be changed to some extent. The deviation of beam orbit also will introduce the variation of field amplitude. In a typical third generation storage ring or DLSR, the beam orbit can be controlled on the level of micron. On this condition, the influence from orbit deviation is small.

Most of the low heat-load undulators are inherited from the APPLE-type undulator. Without considering the adjustability of the polarization state, a non-negligible disadvantage of these undulators is that the horizontal magnetic field is weaker than the vertical magnetic field, which will result in a relatively weak heat-load suppression for the vertical polarization. It is due to an innate defect that the horizontal field or knot field is generated from the out row of undulators. The merged APPLE-Knot undulator can improve the effectiveness of heat-load suppression on vertical mode to some extent. However, its magnet structure is complicated. The correction of field error and the shimming of the tilt magnetization pole will be challenging, and possibly constitute an obstacle to carrying on such an undulator in practice, especially for a DLSR. The on-axis heat load of the vertically polarized radiation is also not completely suppressed [13]. The recently proposed DELTA-Knot undulator also can improve the horizontal magnetic field to some extent by using the DELTA structure with tilt magnetization [25]. However, the vertical polarization degree of the DELTA-Knot undulator is relatively low and its circular mode still has a portion of heat load on the axis. The proposed AMPU takes the advantage of DELTA-type magnet arrangement and can effectively improve the horizontal field so that the on-axis heat load is low both in the horizontal and vertical polarization cases. It is particularly beneficial for a DLSR in which both the horizontal and vertical beam sizes are small. In contrast, the APPLE-type undulator leaves an open gap in the horizontal plane so that in a typical third generation storage ring it is more flexible than the proposed AMPU.

In the proposed two novel undulators, the on-axis heat load within the pinhole radius of $2\sigma'_r$ can be effectively suppressed, and the polarization degrees of different working modes are always on the level of 99%. Most of the heat load is scattered away from the axis. For a normal planar undulator under the same condition, the on-axis power is at least 1 or 2 orders of magnitude larger than the proposed undulators. The effectiveness of heat-load suppression in the proposed undulator also will become more notable for a long undulator length and/or a high-energy storage ring and/or a DLSR. However, the proposed undulator still has some status that probably cannot suppress the on-axis heat load, such as the transition state between the linear mode and circular mode. Even if the undulator can fast change the polarization mode, it is still necessary to evaluate whether the cooling system of optic components can overcome the transient heavy heat load. Therefore, in the proposed undulator, the heat-load problem also should be carefully treated.

V. SUMMARY

This paper proposes a new class of undulators by applying a different period length in each direction based on AMPU with the arrangement of the DELTA/APPLE-X structure. The Figure 8/Knot AMPU is demonstrated by setting the one-to-two/two-to-three period ratio in each direction. Both the linear and circular polarization states can achieve a high polarization degree with the on-axis heat load greatly suppressed. Since the amplitude of the horizontal magnetic field is the same as the vertical magnetic field, here the linear polarized radiation at two predetermined orthogonal directions is almost the same except for the rotated angular distribution of the flux and power. The effectiveness of heat-load suppression and the polarization characteristics at fundamental photon energy for these two novel undulators are on the same level. The novel Knot undulator almost has the same photon flux with the linear mode of the novel Figure 8 undulator, and the circular mode of the novel Figure 8 undulator is about 2 times larger than the others. The major difference is that the Knot undulator has more harmonic components and a higher polarization degree at harmonic than Figure 8 undulator. Moreover, with the increase of harmonic order, the linear polarization direction of Knot undulator is alternately switched between two predetermined orthogonal directions, while in the Figure 8 undulator the polarization direction at harmonic is constant and the polarization degree is deteriorated. Both these two novel undulators are not sensitive to the deviations of phase shift and field amplitude.

The theoretical studies indicate that these two novel types of low heat-load undulators have the potential to satisfy most of the experiment users on heat-load suppression. In this paper, the proposed two novel undulators are taken as examples, other types of fields are also possible to be obtained when utilizing AMPU structure with a different period ratio/phase shift/field amplitude. For example, we can easily obtain the quasiperiodic fields by applying the AMPU concept to each direction, then all the harmonics at an arbitrary polarization state are possible to be shifted to the noninteger multiple of fundamental photon energy. We hope the proposed new class of undulators can offer some new choices for the experiment user to obtain the undulator radiation with a specific feature.

APPENDIX: ELECTRON MOTION IN AMPU

In a AMPU with period ratio of $n_1 : n_2$ between the upper (right) and lower (left) magnet poles, the magnetic field on the axis can be described as

$$\boldsymbol{B}(z) = \left\{ B_1 \sin\left(\frac{k_u z}{n_1} + \phi_3\right) + B_2 \sin\left(\frac{k_u z}{n_2} + \phi_4\right), B_1 \sin\left(\frac{k_u z}{n_1} + \phi_1\right) + B_2 \sin\left(\frac{k_u z}{n_2} + \phi_2\right), B_z \right\} \tag{A1}$$

where $k_u = 2\pi/\lambda_u$ is the wave number. For an electron passing through the undulator with the Lorentz factor γ and average relative velocity β_0, the fundamental angular frequency ω_0 is $k_u \beta_0 c (1 - \frac{K_1^2 + K_2^2}{2\gamma^2})$. In fact, the magnetic field strength B_z along the propagation direction of AMPU is not vanished on the axis, and is comparative to B_x and B_y. However, in a synchrotron radiation light source, the transverse velocities of the electron are about 3–4 orders smaller than the longitudinal velocity, B_z has little contribution to the radiation performance. Therefore it is reasonable to ignore B_z here. The undulator strength parameter is defined as

$$K_{1,2} = \frac{e B_{1,2} n_{1,2} \lambda_u}{2\pi m_0 c}, \tag{A2}$$

where m_0 is the mass of electron, e is the charge of electron and c is the light speed.

Solving the equations of motion under $\gamma m_0 \mathrm{d}\boldsymbol{\beta}/\mathrm{d}t = -e\boldsymbol{\beta} \times \boldsymbol{B}$, we obtain the relative velocity of electron in the undulator as

$$\boldsymbol{\beta}(t) = \left\{ \begin{array}{l} \frac{K_1}{\gamma}\cos\left(\frac{\omega_0}{n_1}t + \phi_1\right) + \frac{K_2}{\gamma}\cos\left(\frac{\omega_0}{n_2}t + \phi_2\right), \\[2mm] \frac{K_1}{\gamma}\cos\left(\frac{\omega_0}{n_1}t + \phi_3\right) + \frac{K_2}{\gamma}\cos\left(\frac{\omega_0}{n_2}t + \phi_4\right), \\[2mm] \beta_0\left\{ 1 - \frac{1}{4\gamma^2\beta_0^2}\left[2K_1^2 + 2K_2^2 + K_1^2\cos\left(\frac{2\omega_0}{n_1}t + 2\phi_1\right) + K_2^2\cos\left(\frac{2\omega_0}{n_2}t + 2\phi_2\right) \right.\right. \\[2mm] \left. + K_1^2\cos\left(\frac{2\omega_0}{n_1}t + 2\phi_3\right) + K_2^2\cos\left(\frac{2\omega_0}{n_2}t + 2\phi_4\right) \right] \\[2mm] - \frac{K_1 K_2}{2\gamma^2\beta_0^2}\left[\cos\left(\frac{\omega_0}{n_1}t + \frac{\omega_0}{n_2}t + \phi_1 + \phi_2\right) + \cos\left(\frac{\omega_0}{n_1}t - \frac{\omega_0}{n_2}t + \phi_1 - \phi_2\right) \right. \\[2mm] \left.\left. + \cos\left(\frac{\omega_0}{n_1}t + \frac{\omega_0}{n_2}t + \phi_3 + \phi_4\right) + \cos\left(\frac{\omega_0}{n_1}t - \frac{\omega_0}{n_2}t + \phi_3 - \phi_4\right) \right]\right\} \end{array} \right. \tag{A3}$$

The position of the electron can be derived by the integral of relative velocity so that

$$\boldsymbol{r}(t) = \left\{ \begin{array}{l} \frac{n_1 K_1 c}{\gamma \omega_0}\sin\left(\frac{\omega_0}{n_1}t + \phi_1\right) + \frac{n_2 K_2 c}{\gamma \omega_0}\sin\left(\frac{\omega_0}{n_2}t + \phi_2\right), \\[2mm] \frac{n_1 K_1 c}{\gamma \omega_0}\sin\left(\frac{\omega_0}{n_1}t + \phi_3\right) + \frac{n_2 K_2 c}{\gamma \omega_0}\sin\left(\frac{\omega_0}{n_2}t + \phi_4\right), \\[2mm] \beta_0 c\left\{ t - \frac{1}{4\gamma^2\beta_0^2}\left[2t K_1^2 + 2t K_2^2 + \frac{n_1 K_1^2}{2\omega_0}\sin\left(\frac{2\omega_0}{n_1}t + 2\phi_1\right) + \frac{n_2 K_2^2}{2\omega_0}\sin\left(\frac{2\omega_0}{n_2}t + 2\phi_2\right) \right.\right. \\[2mm] \left. + \frac{n_1 K_1^2}{2\omega_0}\sin\left(\frac{2\omega_0}{n_1}t + 2\phi_3\right) + \frac{n_2 K_2^2}{2\omega_0}\sin\left(\frac{2\omega_0}{n_2}t + 2\phi_4\right) \right] \\[2mm] - \frac{n_1 n_2 K_1 K_2}{2\omega_0 \gamma^2 \beta_0^2}\left[\frac{1}{(n_2+n_1)}\sin\left(\frac{\omega_0}{n_1}t + \frac{\omega_0}{n_2}t + \phi_1 + \phi_2\right) + \frac{1}{(n_2-n_1)}\sin\left(\frac{\omega_0}{n_1}t - \frac{\omega_0}{n_2}t + \phi_1 - \phi_2\right) \right. \\[2mm] \left.\left. + \frac{1}{(n_2+n_1)}\sin\left(\frac{\omega_0}{n_1}t + \frac{\omega_0}{n_2}t + \phi_3 + \phi_4\right) + \frac{1}{(n_2-n_1)}\sin\left(\frac{\omega_0}{n_1}t - \frac{\omega_0}{n_2}t + \phi_3 - \phi_4\right) \right]\right\} \end{array} \right. \tag{A4}$$

Substituting the one-to-two period ratio and two-to-three period ratio into Eqs. (A3) and (A4), we can obtain the motion equations of electron in the proposed undulators. The radiation characteristics can be calculated based on Eqs. (3)–(5).

———————————

[1] Z. T. Zhao, Storage ring light sources, Rev. Accel. Sci. Techol. **03**, 57 (2010).

[2] M. Eriksson, J. F. Veen, and C. Quitmann, Diffraction-limited storage rings—A window to the science of tomorrow, J. Synchrotron Radiat. **21**, 837 (2014).

[3] C. Feng and H. Deng, Review of fully coherent free-electron lasers, Nucl. Sci. Tech. **29**, 160 (2018).

[4] T. Tanaka and H. Kitamura, Figure-8 undulator as an insertion device with linear polarization and low on-axis power density, Nucl. Instrum. Methods Phys. Res., Sect. A **364**, 368 (1995).

[5] T. Tanaka and H. Kitamura, Analysis of figure-8-undulator radiation, J. Synchrotron Radiat. **3**, 47 (1996).

[6] S. Sasaki, B. Diviacco, and R. P. Walker, Brainstorming on new permanent magnet undulator designs, in *Proceedings of the 6th European Particle Accelerator Conference, Stockholm, 1998* (IOP, London, 1998).

[7] T. Tanaka, T. Hara, M. Oura, H. Ohashi, H. Kimura, S. Goto, Y. Suzuki, and H. Kitamura, Construction and performance of a figure-8 undulator, Rev. Sci. Instrum. **70**, 4153 (1999).

[8] T. Tanaka, K. Shirasawa, and H. Kitamura, Consideration on an undulator magnetic structure for polarization control, Rev. Sci. Instrum. **73**, 1724 (2002).

[9] J. Yan and S. Qiao, Note: Leaf undulator to realize polarization control with low on-axis heat load, Rev. Sci. Instrum. **81**, 056101 (2010).

[10] T. Yamamoto, S. Sasaki, M. Ye, and S. Qiao, Conceptual designs for variably polarizing leaf undulator, AIP Conf. Proc. **2054**, 030026 (2019).

[11] S. Qiao, D. Ma, D. Feng, S. Marks, R. Schlueter, S. Prestemon, and Z. Hussain, Knot undulator to generate linearly polarized photons with low on-axis power density, Rev. Sci. Instrum. **80**, 085108 (2009).

[12] F. Xi, T. Shi, Q. Fan, S. Prestemon, W. Wan, Z. An, and S. Qiao, A preliminary design of a knot undulator, J. Synchrotron Radiat. **20**, 145 (2013).

[13] F. Ji, R. Chang, Q. Zhou, W. Zhang, M. Ye, S. Sasaki, and S. Qiao, Design and performance of the APPLE-Knot undulator, J. Synchrotron Radiat. **22**, 901 (2015).

[14] F. Zhang, Z. Sun, Y. Qiao, and S. Qiao, Practical design and performance of a new merged APPLE-Knot undulator, J. Synchrotron Radiat. **27**, 1494 (2020).

[15] Y. Yang, X. Li, and H. Lu, A practical design and field errors analysis of a merged APPLE-Knot undulator for High Energy Photon Source, Nucl. Instrum. Methods Phys. Res., Sect. A **1011**, 165579 (2021).

[16] Z. Zhao and Q. Jia, Studies on the asymmetric magnet pole undulators, Nucl. Instrum. Methods Phys. Res., Sect. A **999**, 165205 (2021).

[17] A. B. Temnykh, Delta undulator for Cornell energy recovery linac, Phys. Rev. ST Accel. Beams, **11**, 120702 (2008).

[18] A. B. Temnykh, M. Babzien, D. Davis, M. Fedurin, K. Kusche, J. Park, and V. Yakimenko, Delta undulator model: Magnetic field and beam test results, Nucl. Instrum. Methods Phys. Res., Sect. A **649**, 42 (2011).

[19] M. Calvi, C. Camenzuli, E. Prat, and T. Schmidt, Transverse gradient in Apple-type undulators, J. Synchrotron Radiat. **24**, 600 (2017).

[20] T. Schmidt and M. Calvi, APPLE X undulator for the SwissFEL soft X-ray beamline Athos, Synchrotron Radiat. News **31**, 35 (2018).

[21] P. Duke, *Synchrotron Radiation: Production and Properties* (Oxford University Press, New York, 2009).

[22] T. Tanaka and H. Kitamura, SPECTRA: A synchrotron radiation calculation code, J. Synchrotron Radiat. **8**, 1221 (2001).

[23] O. Chubar, P. Elleaume, and J. Chavanne, A three-dimensional magnetostatics computer code for insertion devices, J. Synchrotron Radiat. **5**, 481 (1998).

[24] Z. H. Bai, G. W. Liu, T. L. He, T. Zhang, W. W. Li, P. H. Yang, Z. L. Ren, S. C. Zhang, W. M. Li, G. Y. Feng, and L. Wang, A modified hybrid 6BA lattice for the HALF storage ring, in *Proceedings of the IPAC2021, Campinas, SP* (JACoW, Campinas, SP, Brazil, 2021), pp. 407–409, MOPAB112.

[25] X. Y. Li, H. H. Lu, and S. C. Sun, Physical design of a cryogenic delta-knot undulator for the High Energy Photon Source, Nucl. Instrum. Methods Phys. Res., Sect. A **986**, 164639 (2021).